

*t*P40 carbon: A novel superhard carbon allotrope

Heng Liu(刘恒), Qing-Yang Fan(樊庆扬), Fang Yang(杨放), Xin-Hai Yu(于新海), Wei Zhang(张伟), Si-Ning Yun(云斯宁)

Citation: Chin. Phys. B . 2020, 29(10): 106102 . **doi:** 10.1088/1674-1056/ab9c01
Journal homepage: http://cpb.iphy.ac.cn; http://iopscience.iop.org/cpb

What follows is a list of articles you may be interested in

Quantum density functional theory studies of structural, elastic, and opto-electronic properties of $ZMoO_3$ (*Z*=Ba and Sr) under pressure

Saad Tariq, A A Mubarak, Saher Saad, M Imran Jamil, S M Sohail Gilani

Chin. Phys. B . 2019, 28(6): 066101 . **doi:** 10.1088/1674-1056/28/6/066101

Ab-initio investigation of $AGeO_3$ (*A*=Ca, Sr) compounds via Tran–Blaha-modified Becke–Johnson exchange potential

Rasul Bakhsh Behram, M A Iqbal, Muhammad Rashid, M Atif Sattar, Asif Mahmood, Shahid M Ramay

Chin. Phys. B . 2017, 26(11): 116103 . **doi:** 10.1088/1674-1056/26/11/116103

High-pressure structure and elastic properties of tantalum single crystal: First principles investigation

Jian-Bing Gu(顾建兵), Chen-Ju Wang(王臣菊), Wang-Xi Zhang(张旺玺), Bin Sun(孙斌), Guo-Qun Liu(刘国群), Dan-Dan Liu(刘丹丹), Xiang-Dong Yang(杨向东)

Chin. Phys. B . 2016, 25(12): 126103 . **doi:** 10.1088/1674-1056/25/12/126103

Theoretical calculations of structural, electronic, and elastic properties of $CdSe_{1-x}Te_x$: A first principles study

M Shakil, Muhammad Zafar, Shabbir Ahmed, Muhammad Raza-ur-rehman Hashmi, M A Choudhary, T Iqbal

Chin. Phys. B . 2016, 25(7): 076104 . **doi:** 10.1088/1674-1056/25/7/076104

Theoretical investigation of sulfur defects on structural, electronic, and elastic properties of ZnSe semiconductor

Muhammad Zafar, Shabbir Ahmed, M. Shakil, M. A. Choudhary, K. Mahmood

Chin. Phys. B . 2015, 24(7): 076106 . **doi:** 10.1088/1674-1056/24/7/076106

---

*t*P40 carbon: A novel superhard carbon allotrope*

Heng Liu(刘恒)[1], Qing-Yang Fan(樊庆扬)[1,†], Fang Yang(杨放)[1],
Xin-Hai Yu(于新海)[2], Wei Zhang(张伟)[3], and Si-Ning Yun(云斯宁)[4,‡]

[1] *College of Information and Control Engineering, Xi'an University of Architecture and Technology, Xi'an* 710055, *China*
[2] *Department of Mechanical and Electrical Engineering, Hetao College, Bayannur Inner Mongolia* 015000, *China*
[3] *School of Microelectronics, Xidian University, Xi'an* 710071, *China*
[4] *Functional Materials Laboratory, School of Materials Science and Engineering, Xi'an University of Architecture and Technology, Xi'an* 710055, *China*

(Received 9 March 2020; revised manuscript received 25 May 2020; accepted manuscript online 12 June 2020)

In this work, a novel carbon allotrope *t*P40 carbon with space group $P4/mmm$ is proposed. The structural stability, mechanical properties, elastic anisotropy, and electronic properties of *t*P40 carbon are investigated systematically by using density functional theory (DFT). The calculated elastic constants and phonon dispersion spectra indicate that the *t*P40 phase is a metastable carbon phase with mechanical stability and dynamic stability. The B/G ratio indicates that *t*P40 carbon is brittle from 0 GPa to 60 GPa, while *t*P40 carbon is ductile from 70 GPa to 100 GPa. Additionally, the anisotropic factors and the directional dependence of the Poisson's ratio, shear modulus, and Young's modulus of *t*P40 carbon at different pressures are estimated and plotted, suggesting that the *t*P40 carbon is elastically anisotropic. The calculated hardness values of *t*P40 carbon are 44.0 GPa and 40.2 GPa obtained by using Lyakhov–Oganov's model and Chen's model, respectively, which means that the *t*P40 carbon can be considered as a superhard material. The electronic band gap within Heyd–Scuseria–Ernzerhof hybrid functional (HSE06) is 4.130 eV, and it is found that the *t*P40 carbon is an indirect and wider band gap semiconductor material.

Keywords: novel carbon allotrope, elastic properties, anisotropy, superhard material

PACS: 61.50.Ah, 61.50.–f, 71.20.Nr, 71.55.Cn **DOI:** 10.1088/1674-1056/ab9c01

1. Introduction

Carbon can be widely found in the air and in Earth's crust in diverse forms; it can chemically self-associate, forming three flexible hybridization bonds (sp, sp^2, and sp^3) in diamond, graphite, and other carbon allotropes.[1–36] Carbon allotropes play increasingly a critical role in biology and commerce due to their complex structures and diverse properties, which are a hot research topic.

A considerable research has predicted the properties of many carbon allotropes in recent years. For example, all-sp^3 hybrid carbon allotropes incorporate *Z* carbon,[21] *T*E-C36 carbon,[22] *K*6 carbon,[23] *Cmmm*-C_{32} and $P6/mmm$-C_{54},[24] and other hybridized carbons include *m*C16,[25] *H*18 carbon,[26] and *m*C12.[27] In addition, several novel superhard carbon materials have also been predicted in recent years, such as *bct*-C4,[28] *O*-carbon,[29] C14 carbon,[30] and *Amm*2-carbon.[31,32] Previous research by Li *et al.*[33] identified a new carbon allotrope, denoted as C_{96} carbon, with a porous nanocube network. The calculated bulk modulus and hardness of C_{96} carbon (279 GPa and 25 GPa) are higher than those of T carbon,[34] and it was found that C_{96} carbon can be considered as a semiconductor material with an indirect band gap of 1.85 eV. Wang *et al.*[35] proposed a cubic sp^3hybridized carbon material called C_{20}–T carbon, they found that C_{20}–T carbon has a high hardness (72.76 GPa) and it is a transparent insulator with an indirect band gap 5.44 eV. In addition, the interesting structure of C_{20}–T carbon has large cavities with a diameter of about 3 Å. A potential superhard carbon material $P2/m$ C_{54} was proposed by Li and Xing.[36] The $P2/m$ C_{54} remains stable mechanically and dynamically at 100 GPa, and the relative formation enthalpy of $P2/m$ C_{54} was calculated to be higher 0.581 eV/atom than that of graphite, and it is less 0.729 eV/atom than that of T carbon, and T carbon has already synthesized by Zhang *et al.*[37] According to Chen *et al.*'s model[38] and Lyakhov and Oganov's model,[39] the obtained hardness of $P2/m$ C_{54} is 54.1 GPa and 70.4 GPa, which reveals its superhard characteristics. In addition, Zhang *et al.*[24] predicted two new carbon allotropes (*Cmmm*-C_{32} and $P6/mmm$-C_{54}) with a full sp^3 bonding network, both of these new carbon materials have honeycomb structures. By using Lyakhov–Oganov model,[39] the hardness values of *Cmmm*-C_{32} and $P6/mmm$-C_{54} were estimated to be 83.72 GPa and 54.01 GPa, respectively, indicating that they are identified to be superhard materials.

*Project supported by the National Natural Science Foundation of China (Grant Nos. 61804120 and 61901162), the China Postdoctoral Science Foundation (Grant Nos. 2019TQ0243 and 2019M663646), the Young Talent Fund of University Association for Science and Technology in Shaanxi Province, China (Grant No. 20190110), the National Key Research and Development Program of China (Grant No. 2018YFB1502902), and the Key Program for International Science and Technolog Cooperation Projects of Shaanxi Province, China (Grant No. 2019KWZ-03).

†Corresponding author. E-mail: qyfan_xidian@163.com; fanqy@xauat.edu.cn
‡Corresponding author. E-mail: alexsyun1974@aliyun.com; yunsining@xauat.edu.cn

© 2020 Chinese Physical Society and IOP Publishing Ltd

In this work, based on first-principles calculations, a novel carbon allotrope, which is called *t*P40 carbon, is predicted to possess the space group $P4/mmm$ in sp^3 bonding networks by space group and graph theory (RG2).[40,41] The *t*P40 carbon is not included in SACADA[42] (http://sacada.sctms.ru), nor Materials Project (https://materialsproject.org/), nor Reticular Chemistry Structure Resource (RCSR,[43,44] http://rcsr.net/). The crystal structure of *t*P40 carbon is similar to that of P carbon.[45] The structural stability, anisotropic and electronic properties of *t*P40 carbon are investigated systematically.

2. Computational details and theory

The structural optimization and property calculations of *t*P40 carbon were completed by using density functional theory (DFT)[46,47] as implemented in the Cambridge Serial Total Energy Package (CASTEP).[48] The exchange–correlation (XC) energy functionals are approximated by the generalized gradient approximation (GGA) parameterized by Perdew, Burke and Ernzerr (PBE)[49] and local density approximation (LDA).[50] The electronic properties were investigated by utilizing the Heyd–Scuseria–Ernzerhof hybrid functional (HSE06).[51] In this work, the energy cut-off is 400 eV for the *t*P40 carbon. The Brillouin zone is sampled with a 5×5×9 Monkhorst–Pack special *k*-point grid. Vanderbilt ultrasoft pseudopotential[52] is used, and the Broyden–Fletcher–Goldfarb–Shanno (BFGS)[53] minimization scheme is utilized for optimizing the structural geometry. The phonon spectra of *t*P40 carbon under 0 GPa and 100 GPa are found by adopting the density functional perturbation theory (DFPT) approach[54] The convergence of the total energy difference is less than 5×10^{-6} eV/atom, the maximum Hellmann–Feynman force is 0.01 eV/Å, and the self-consistent field tolerance threshold is 5×10^{-7} eV/atom. When the crystal structure under high pressure is optimized, the applied pressure is hydrostatic pressure. The elastic constants are calculated by the strain–stress method.

3. Results and discussion

3.1. Structural properties

The crystal structure of *t*P40 carbon is presented in Fig. 1. From Fig. 1, it is found that *t*P40 carbon consists of five nonequivalent carbon atoms with the space group $P4/mmm$. C1, C2, C3, C4, and C5 are each depicted in a different colour. The *t*P40 carbon has 40 carbon atoms in each conventional cell occupying five different Wyckoff positions: C1 8*t* (1.13577, 1.5, 0.32069), C2 4*o* (1.5, 1.28224, 1.5), C3 4*k* (1.66058, 1.33942, 0.5), C4 8*r* (1.22628, 1.77372, 0.32633), and C5 16*u* (1.09773, 1.66284, 0.17872), and the details are shown in Fig. 1(c). It is found that the minimum bond length of *t*P40 carbon is 1.434 Å, the maximum bond length is 1.644 Å, the average bond length of C–C is 1.541 Å, and it is slightly smaller than that diamond (1.544 Å). The primary reason is the bond length of the three-membered ring consisting of C1 and C2 in Fig. 1(b) (the bond length of C1–C2 is 1.462 Å) and the eight-membered ring consisting of C2 and C3 (the bond length of C2–C3 is 1.434 Å) located in the middle of Fig. 1(c) are shorter. From Figs. 1(b) and 1(c), one can see that the *t*P40 carbon has a three-membered ring, five-membered ring, six-membered ring, eight-membered ring, and twelve-membered ring, and there is only one kind of them except for the three-membered ring. The five-membered ring consists of the C1, C2, C3, C4, and C5 atoms. The six-membered ring comprises two kinds of atoms: C1 and C4. The eight-membered ring is made up of C2 and C3 atoms. The twelve-membered ring is composed of C4 and C5 atoms. While three-membered ring consists of the C1+C2 atoms, and another way to form it is C2+C4 atoms (see Fig. 1(b)). The crystal structure of *t*P40 carbon is similar to that of P carbon,[45] and the crystal structure of P carbon is shown in Fig. 1(d).

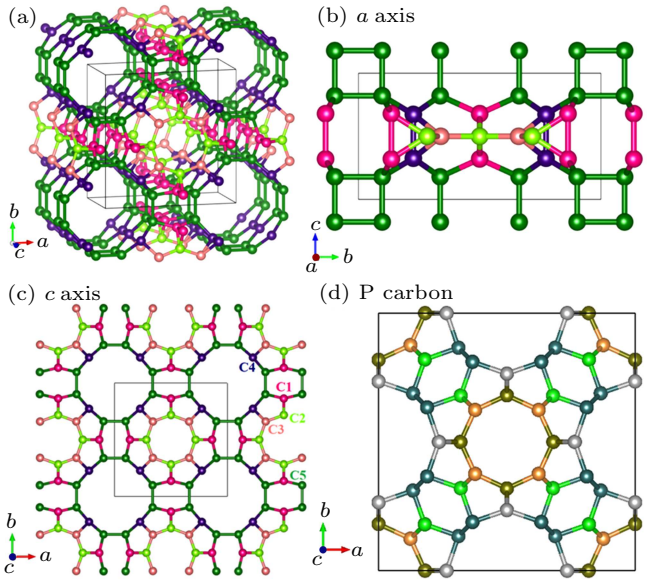


Fig. 1. Crystal structure of *t*P40 carbon (a) along the *a* axis (b) and *b* axis (c), and crystal structure of P carbon (d).

In this work, the calculated lattice constants of *t*P40 carbon within GGA and LDA, together with those of C_{96}, *Pnma*-BN,[55] C_{64},[56] C72,[57] and diamond, are listed in Table 1. Under an ambient pressure, the lattice parameters for *t*P40 carbon are $a = 8.414$ Å and $c = 4.383$ Å in a conventional cell. When using different methods to calculate the lattice parameters of diamond, the GGA level is closer to the experimental value, so all the discussion in this work is based on the results of GGA level. The calculated results show that the volumes per carbon atom of *t*P40 carbon, C_{64}, C72, and diamond are 7.756 Å^3, 6.022 Å^3, 11.760 Å^3, and 11.341 Å^3, respectively. In addition, the obtained density of *t*P40 carbon is 2.571 g/cm^3, which is lower than that of C_{96} (2.700 g/cm^3)[33] and slightly higher than that of C_{64} (2.562 g/cm^3)[56] and C72 (1.690 g/cm^3).[57]

Table 1. Calculated values of lattice constant (in unit Å), cell volume (in unit Å^3), and density (in unit g/cm^3) for *t*P40 carbon, C_{64}, *Pnma*-BN, C_{96}, and diamond.

Crystal	Method	*a*	*b*	*c*	*V*	*ρ*
*t*P40 carbon	GGA[a]	8.414		4.383	7.756	2.571
	LDA[a]	8.314		4.329	7.482	2.666
C_{64}		7.180[b]		2.511	6.022	2.562
Pnma-BN	GGA[c]	4.890	2.589	4.284	13.557	
	LDA[c]	4.795	2.557	4.243	13.007	
C_{96}	PW91[d]	9.020				2.700
	GGA[e]	9.004				
C72		9.460[f]			11.760	1.690
Diamond	GGA[a]	3.566			11.341	
		3.566[g]			11.337	
	LDA[a]	3.526			10.961	
		3.525[g]			10.950	
	Exp.[h]	3.567			11.346	

[a]This work, [b]Ref. [56], [c]Ref. [55], [d]Ref. [33], [e]Ref. [58], [f]Ref. [57], [g]Ref. [59], [h]Ref. [60].

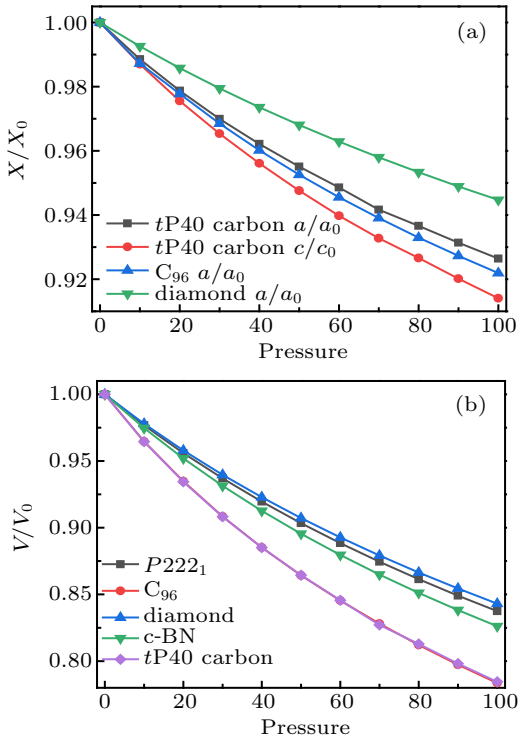


Fig. 2. Plots of ratios of (a) a/a_0, c/c_0 and (b) V/V_0 *versus* pressure for *t*P40 carbon, C_{96} carbon, $P222_1$ carbon, c-BN carbon, and diamond.

The ratios of a/a_0, c/c_0, and V/V_0 each as a function of pressure for *t*P40 carbon, C_{96}, $P222_1$, c-BN, and diamond are plotted in Fig. 2, where a_0, c_0, and V_0 are the lattice constants and cell volume at zero pressure, respectively. The values of a/a_0, c/c_0, and V/V_0 for these materials decrease at different rates as the pressure increases. There is no doubt that diamond is the most difficult to compress carbon material, because its hardness is the highest in nature. The values of a/a_0 and c/c_0 can be related to the compressibility of material. Thus, when hydrostatic pressure is applied to *t*P40 carbon, it is more easily compressed along the *c* axis. From Fig. 2(a), it can be easily seen that the a/a_0 ratio of *t*P40 carbon is larger than that of C_{96}, which indicates that *t*P40 carbon is less likely to be compressed along the *a* axis than C_{96}, when subjected to hydrostatic pressure. As is well known, the value of V/V_0 is related to the bulk modulus of the material, and the curve of diamond is the highest in all the materials under study here, so its bulk modulus is the largest. Apparently, the volume ratio V/V_0 of *t*P40 carbon is smaller than that of c-BN and $P222_1$ carbon. Therefore, it can be predicted that the bulk modulus of *t*P40 carbon is smaller than that of c-BN carbon and $P222_1$ carbon.

3.2. Elastic properties

To study the mechanical properties of *t*P40 carbon, the elastic constants C_{ij}, the bulk modulus, shear modulus, and Young's modulus for each of *t*PC_{40} carbon, C_{64}, *Pnma*-BN, C_{96}, C72, and diamond are presented in Table 2. According to the elastic constants (C_{11}, C_{12}, C_{13}, C_{33}, C_{44}, C_{66}) given in Table 2, the mechanically stability of *t*P40 carbon can be estimated based on the criteria as follows: $C_{11} > |C_{12}|$, $2C_{13}^2 < C_{33}(C_{11}+C_{12})$, $C_{44} > 0$, $C_{66} > 0$.[61] The calculated results show that the elastic constants satisfy the mechanical stability criteria. Therefore, *t*P40 carbon is mechanically stable under ambient pressure. To obtain more information about dynamical stability, the phonon spectra for *t*P40 carbon at 0 GPa and 100 GPa are shown in Fig. 3. There is no imaginary frequency in the whole Brillouin zone, which indicates that *t*P40 carbon is dynamically stable at 100 GPa.

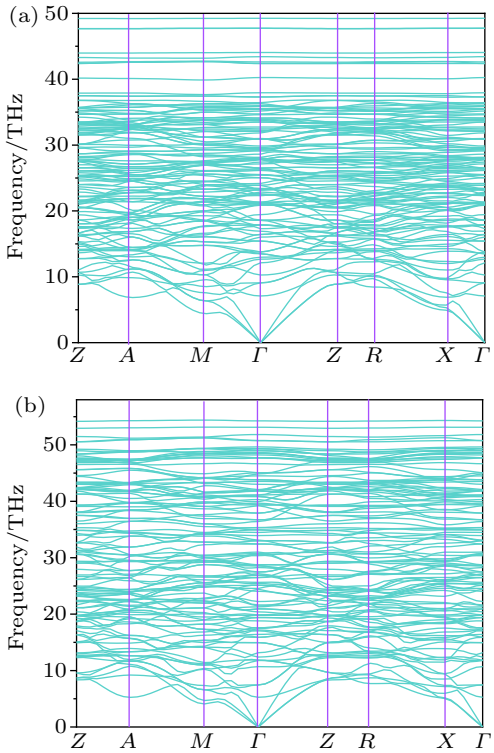


Fig. 3. Phonon spectra for *t*P40 carbon at (a) 0 GPa and (b) 100 GPa.

Voigt states that the Voigt bond is the upper limit of the actual polycrystalline constant, whereas the Reuss bound is the lower limit. Based on the Hill approximation, the values

of the bulk modulus B and the shear modulus G are equal to the arithmetic mean of the Voigt and Reuss and are expressed as[63] $G=(G_R+G_V)/2$ and $B=(B_R+B_V)/2$. The calculated results show that the bulk modulus of tP40 carbon (259 GPa) is larger than that of C72 (183 GPa) and slightly smaller than that of C_{64} (264 GPa), *Pnma*-BN (298 GPa), P carbon (334 GPa), and C_{96} (279 GPa). The value of B for tP40 carbon is about 66.4% of the bulk modulus for diamond (431 GPa). Of all the materials under study, C72 has the lowest bulk modulus. Additionally, it can be observed that the tP40 carbon has a higher shear modulus than the other four carbon materials except for diamond and P carbon, and the shear modulus of C72 is still the lowest. Young's modulus and Poisson's ratio are given by $E=9BG/(3B+G)$ and $v=(3B-2G)/[2(3B+G)]$.[63–65] The calculated Young's modulus of tP40 carbon is 540 GPa, which is greater than that of C_{64} by approximately 5.88%, C_{96} by approximately 3.65%, C72 by approximately 172.72%, and slightly smaller 3 GPa than that of *Pnma*-BN. By using Chen's model[38] and Lyakhov–Oganov's model,[39] the hardness of tP40 carbon is 40.2 GPa and 44.0 GPa, respectively, slightly harder than that of *Pnma*-BN (33.0 GPa using Lyakhov–Oganov's model, which is in excellent agreement with the reported 33.3 GPa[55]). Thus, it can be considered to be a superhard carbon material. The value of v for the tP40 carbon is 0.152 within GGA, which is lower than that of C72 (0.310) and C_{64} (0.178) and higher than that of diamond (0.070). According to Pugh's research,[66] the ratio of bulk to shear modulus (B/G) can be naturally related to the brittleness and ductility of crystal. If $B/G>1.75$, the material is usually ductile; otherwise, it is brittle. The calculated B/G ratios of tP40 carbon under different pressures are listed in Table 3. In the case of tP40 carbon, the calculated results suggest that the tP40 carbon is brittle from 0 GPa to 60 GPa and that when the pressure exceeds 70 GPa, the tP40 carbon becomes ductile.

The elastic constants, bulk modulus B, shear modulus G, and Young's modulus E under pressures from 0 GPa to 100 GPa are illustrated in Fig. 4. In general, the elastic parameters of bulk modulus, shear modulus, and Young's modulus all increase at different rates as the pressure increases. The C_{44} and C_{66} of tP40 carbon increase slowly, whereas the C_{11} and C_{12} increase faster than the other parameters. The degree of dependence of the elastic parameters B, G, and E on pressure are calculated to be 3.36, 0.45, and 1.84, respectively, which indicates that the tP40 carbon has the fastest increase in bulk modulus and the slowest increase in shear modulus.

Table 2. Calculated values of elastic constants of C_{ij} (in unit GPa), bulk modulus B (in unit GPa), shear modulus G (in unit GPa), Young's modulus E (in unit GPa), Poisson's ratio v, and B/G ratio for each of tP40 carbon, C_{64}, *Pnma*-BN, C_{96}, C72, and diamond.

	tP40	C_{64}[a]	*Pnma*-BN[b]	C_{96}[c]	C72[d]	P carbon[e]	Diamond	Diamond[f]
C_{11}	542	598	392	623	273	754	1053	1076
C_{12}	174		99	108	139	152	120	125
C_{13}	82		256			56		
C_{22}			770					
C_{23}			116					
C_{33}	575	677	675			979		
C_{44}	240	254	299	194	81	401	563	577
C_{55}			272					
C_{66}	261		187			285		
B	259	264	298	279	183	334	431	442
G	234	217	227	219	75	360	522	
E	540	510	543	521	198	795	1116	
v	0.152	0.178			0.310	0.104	0.070	
B/G	1.106	1.220			2.46	0.928	0.826	

[a]Ref. [56], [b]Ref. [55], [c]Ref. [33], [d]Ref. [57], [e]Ref. [45], [f]Ref. [62]-experimental.

The elastic Debye temperature Θ_D and the average sound velocity v_m are related by the expression[67,68] $\Theta_D=v_m(h/k_B)[3n/(4\pi)(N_A\rho/M)]^{1/3}$, where k is Boltzmann's constant, h is Planck's constant, n is the number of atoms in the molecule, N_A is Avogadro's number, ρ is the density, and M is the molecular weight. Additionally, $v_m=[(2/v_s^3+1/v_p^3)/3]^{-1/3}$. The values of shear wave velocity (v_s) and compressional wave velocity (v_p) are estimated from Navier's equations: $v_s=(G/\rho)^{1/2}$ and $v_p=[(B+4G/3)/\rho]^{1/2}$. The calculation results of the average sound velocity, compressional and shear wave velocities, Debye temperature Θ_D, and B/G ratio results for tP40 carbon at different pressures are listed in Table 3. It is found that the Debye temperatures of tP40 carbon are 1579 K and 1682 K at 0 GPa and 100 GPa, respectively, and Θ_D generally increases with pressure increasing. The obtained Debye temperature of *Pnma*-BN is determined to be 1504 K at zero pressure by Ma *et al.*,[55] which is slightly smaller than that of tP40 carbon. Fan *et al.*[69] calculated and discussed the Θ_D of *Pbca*-BN (1734 K), diamond (2230 K),[70] Diamondyne (422 K)[71] at ambient pressure. Of all the materials mentioned in this work, diamond has the highest Θ_D and is the hardest material, and the Debye temperatures

of Diamondyne is the lowest.

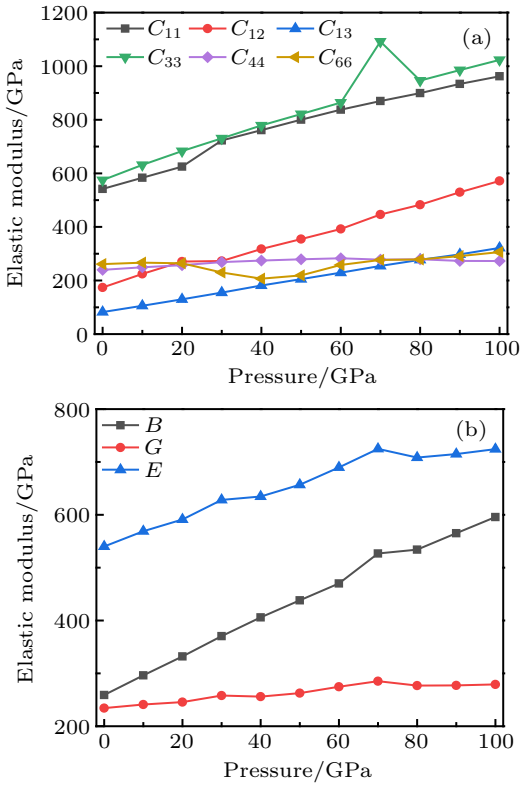


Fig. 4. Plots of (a) elastic constants and (b) B, G, and E for tP40 carbon *versus* pressures.

Table 3. Estimated shear wave velocity (v_s), compressional wave velocity (v_p), average sound velocity v_m, Debye temperature Θ_D, and B/G ratio results for tP40 carbon.

	v_p/(m/s)	v_s/(m/s)	v_m/(m/s)	Θ_D/K	B/G
0	14908	9545	10487	1579	1.106
10	15271	9568	10538	1606	1.229
20	15483	9447	10434	1607	1.352
30	15886	9546	10559	1641	1.435
40	16039	9387	10409	1633	1.586
50	16280	9397	10443	1649	1.668
60	16584	9504	10558	1681	1.712
70	17051	9578	10659	1701	1.847
80	16898	9356	10423	1682	1.929
90	17036	9278	10349	1680	2.039
100	17184	9227	10303	1682	2.134

3.3. Elastic anisotropy

The shear anisotropic coefficient can provide important information concerning the anisotropy of bonding between atoms in different planes. The shear anisotropic coefficient A_1 for the (101) shear plane between [011] and [010] is $A_1 = 4C_{44}/(C_{11}+C_{33}-2C_{13})$;[72] for the (010) shear plane between [101] and [001], $A_2 = 4C_{55}/(C_{22}+C_{33}-2C_{23})$;[72] and for the (001) shear plane between [110] and [010], $A_3 = 4C_{66}/(C_{11}+C_{22}-2C_{12})$.[72] The anisotropy of the bulk modulus along the a axis and c axis relative to that along the b axis are taken as $A_{Ba} = B_a/B_b$ and $A_{Bc} = B_c/B_b$,[73] respectively. The bulk modulus along the a axis, b axis, and c axis are B_a, B_b, and B_c, respectively, which can be given by[73] $B_a = \Lambda/(1+\alpha+\beta)$, $B_b = B_a\alpha$, and $B_c = B_a/\beta$, whereas $\Lambda = C_{11}+2C_{12}+C_{22}\alpha^2+2C_{13}\beta+C_{33}\beta^2+2C_{23}\alpha\beta$, $\alpha = [(C_{11}-C_{12})(C_{33}-C_{13})-(C_{23}-C_{13})(C_{11}-C_{13})]/[(C_{33}-C_{13})(C_{22}-C_{12})-(C_{13}-C_{23})(C_{11}-C_{13})]$, and $\beta = [(C_{22}-C_{12})(C_{11}-C_{13})-(C_{11}-C_{12})(C_{23}-C_{12})]/[(C_{22}-C_{12})(C_{33}-C_{13})-(C_{12}-C_{23})(C_{13}-C_{23})]$. The calculated anisotropy factors A_1, A_3, B_a, B_c, A_{Ba}, and A_{Bc} are listed in Table 4. The values of shear anisotropic coefficients A_1, A_2, and A_3 are important indices to measure whether the crystal has anisotropy. If A_1, A_2, and A_3 are all equal to 1, then the material is isotropic; otherwise, it is anisotropic. Our results indicate that the tP40 carbon is an elastic anisotropic crystal. The shear anisotropic factor A_1 decreases by 19.35% from 0 GPa to 100 GPa, and shear anisotropic factor A_3 deceases from 0 GPa to 40 GPa, but increases from 50 GPa to 100 GPa. Apparently, the bulk modulus along the a-axis B_a has the same value along the b-axis B_b, and B_a and B_c both increase with pressure rising. The obtained directional bulk modulus B_a is greater than B_c, which means that the compressibility along the c axis is the largest. The estimated anisotropy of the bulk modulus along the a-axis A_{Ba} is equal to 1 at all pressures. The values of A_{Bc}, which represent the anisotropy of the bulk modulus along the b axis and c axis, decrease with pressure increasing, while it reaches a maximum value at 70 GPa.

Table 4. Anisotropy factors of tP40 carbon from 0 GPa to 100 GPa.

Pressure	A_1	A_3	B_a	B_c	A_{Ba}	A_{Bc}
0	1.008	1.421	807.58	721.47	1.00	0.893
10	0.994	1.487	928.01	817.32	1.00	0.881
20	0.981	1.491	1044.87	908.75	1.00	0.870
30	0.940	1.022	1179.82	990.59	1.00	0.840
40	0.932	0.932	1295.93	1081.51	1.00	0.835
50	0.922	0.984	1403.18	1160.81	1.00	0.827
60	0.910	1.159	1508.43	1241.13	1.00	0.823
70	0.765	1.307	1561.37	1619.36	1.00	1.037
80	0.865	1.338	1724.73	1394.34	1.00	0.808
90	0.825	1.440	1838.87	1456.74	1.00	0.792
100	0.813	1.567	1942.09	1529.97	1.00	0.788

To visualize and ensure the elastic anisotropy of tP40 carbon, the directional dependence of the shear modulus, Young's modulus, and Poisson's ratio at different pressures are plotted in Fig. 5. The directional dependence of the shear modulus, Young's modulus, and Poisson's ratio are predicted by Elastic Anisotropy Measures (ElAM) code.[74] If a material is isotropic, then its three-dimensional surface constructions of shear modulus, Young's modulus, and Poisson's ratio appear as sphere,[64,75–77] and the measured performance values of the material in different directions are exactly the same, while the degree of deviation from the sphere reflects the strength of anisotropy. It can be clearly seen from Fig. 5 that the three-dimensional surface constructions of Young's modulus under different pressures are not of sphere, which indicates that the materials show anisotropy. When the pressure is 100 GPa,

the three-dimensional shape deviates most from the sphere, indicating that the anisotropy is greater at 100 GPa than that at 0 GPa and 50 GPa. To investigate the elastic anisotropy of *t*P40 carbon in more detail, the maximum, minimum values of Young's modulus, shear modulus, and Poisson's ratio, and $X_{\max}/X_{\min}$ ($X = E$, G, v) of *t*P40 carbon are calculated and listed in Table 5. For anisotropic materials, the maximum and minimum values of Young's modulus, shear modulus, and Poisson's ratio measured in all directions are the same, so the ratio of the maximum value to the minimum value should be 1. The $E_{\max}/E_{\min} = 1.24$, $G_{\max}/G_{\min} = 1.42$, and $v_{\max}/v_{\min} = 3.44$ at ambient pressure, which suggests that the *t*P40 carbon shows elastic anisotropy. It can be seen in Table 5 that as the pressure increases the change of the anisotropy in the shear modulus, Young's modulus, and Poisson's ratio for *t*P40 carbon are irregular. Note that the *t*P40 carbon shows the weakest elastic anisotropy at 30 GPa. Furthermore, the anisotropy in Young's modulus and Poisson's ratio are the largest at 70 GPa, and the anisotropy in Poisson's ratio is the strongest at 100 GPa. The values of $X_{\max}/X_{\min}$ ($X = E$, G, v) for diamond at the ambient pressure is 1.15, 1.21, and 11.00, respectively, which suggests that the *t*P40 carbon exhibits greater elastic anisotropy in Young's modulus and shear modulus and weaker elastic anisotropy in the Poisson's ratio than that of diamond.

To obtain more information about the mechanical anisotropy of Young's modulus, the maximum and minimum Young's modulus, and the value of $E_{\max}/E_{\min}$ in the (100), (010), (011), (101), (001), (110), and (111) planes are shown in Table 6. As is exhibited in Table 6, the maximum and minimum values of Young's modulus are consistent among some planes, such as the (100) and (010) planes, and the (011) and (101) planes. In the range from 0 GPa to 20 GPa, the anisotropy of the Young's modulus is the smallest along the (110) direction and the largest along the (001) direction. However, when the pressure is at 30 GPa, the anisotropy in the Young's modulus is the weakest in the (001) plane and the strongest in the (100) and (010) planes. At zero pressure, the value of $E_{\max}/E_{\min}$ of diamond is 1.11 in the (100), (010), and (001) planes, 1.15 in the (011), (101), and (110) planes, and 1.00 in the (111) plane, indicating that *t*P40 carbon exhibits weaker elastic anisotropy in the (110) plane and stronger anisotropy in the other six mean planes than diamond.

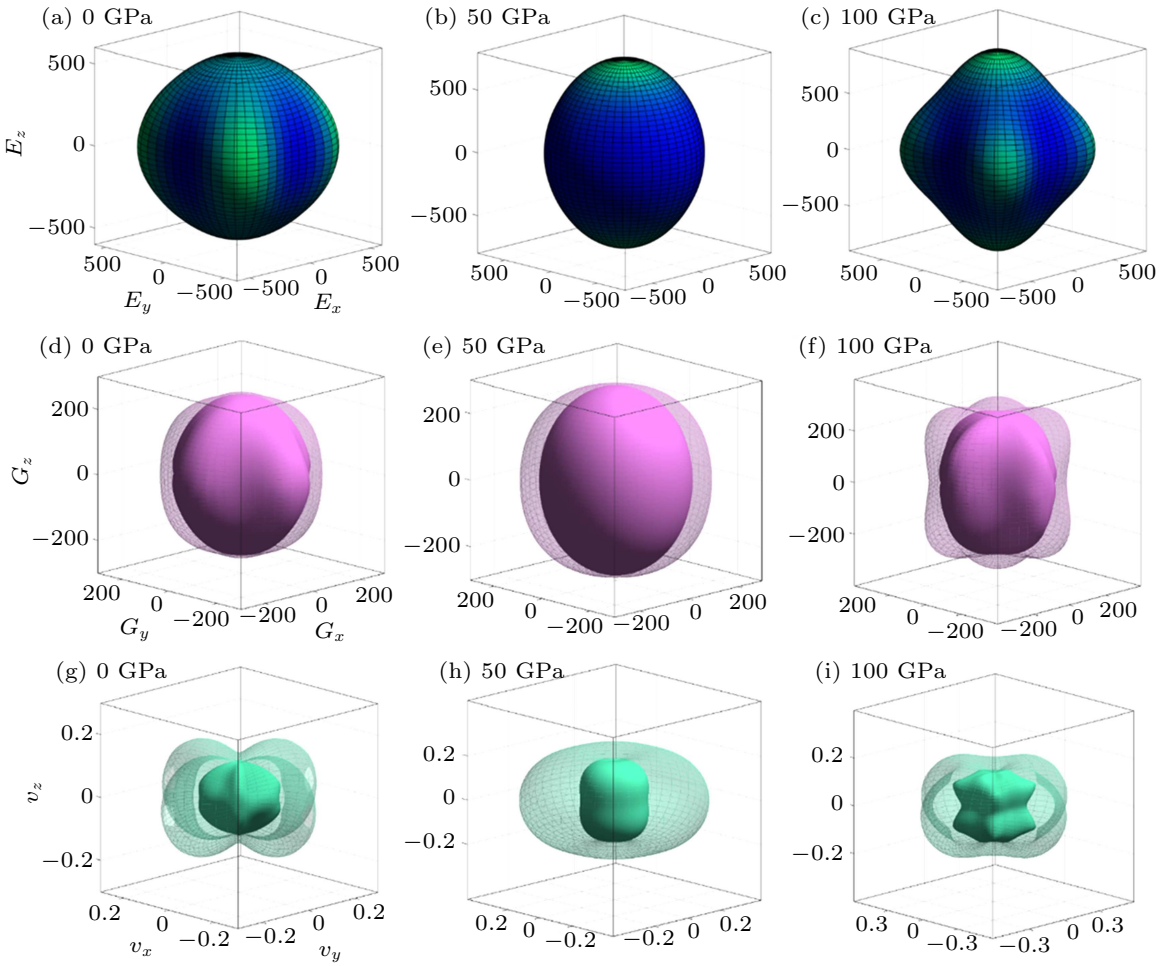


Fig. 5. Directional dependence of Young's modulus at (a) 0 GPa, (b) 50 GPa, and (c) 100 GPa; the shear modulus at (d) 0 GPa, (e) 50 GPa, and (f) 100 GPa; and Passion's ratio at (g) 0 GPa, (h) 50 GPa, and (i) 100 GPa for *t*P40 carbon.

Table 5. Mximum values and minimum values of Young's modulus (in unit GPa), shear modulus (in unit GPa), and Poisson's ratio and E_{max}/E_{min}, G_{max}/G_{min}, and ν_{max}/ν_{min} for *t*P40 carbon.

	E_{max}	E_{min}	Ratio	G_{max}	G_{min}	Ratio	ν_{max}	ν_{min}	Ratio
0	595	480	1.24	261	184	1.42	0.31	0.09	3.44
10	631	490	1.29	272	180	1.51	0.37	0.10	3.70
20	651	500	1.30	283	177	1.60	0.41	0.11	3.73
30	683	607	1.13	282	225	1.25	0.35	0.14	2.50
40	718	584	1.23	286	207	1.38	0.41	0.14	2.93
50	748	619	1.21	293	219	1.34	0.41	0.15	2.73
60	779	635	1.23	314	223	1.41	0.43	0.15	2.87
70	994	626	1.59	368	212	1.74	0.48	0.12	4.00
80	835	621	1.34	335	208	1.61	0.49	0.15	3.27
90	864	615	1.41	348	202	1.72	0.52	0.15	3.47
100	888	604	1.47	358	195	1.84	0.55	0.14	3.92

Table 6. Maximum and minimum Young's moduli and the values of E_{max}/E_{min} in different planes at different pressures for *t*P40 carbon.

P	(100) (010)			(011) (101)			(001)			(110)			(111)		
	E_{max}	E_{min}	Ratio	E_{max}	E_{min}	Ratio	E_{max}	E_{min}	Ratio	E_{max}	E_{min}	Ratio	E_{max}	E_{min}	Ratio
0	555	480	1.16	562	480	1.17	595	480	1.24	595	548	1.09	595	520	1.14
10	604	490	1.23	595	490	1.21	631	490	1.29	631	585	1.08	631	543	1.16
20	645	500	1.29	618	500	1.24	651	500	1.30	651	613	1.06	651	563	1.16
30	683	607	1.13	627	607	1.03	616	607	1.01	683	615	1.11	642	614	1.05
40	718	614	1.17	645	607	1.06	614	584	1.05	718	584	1.23	660	584	1.13
50	748	626	1.19	662	626	1.06	626	619	1.01	748	619	1.21	683	619	1.10
60	779	635	1.23	688	635	1.08	704	635	1.11	779	688	1.17	710	665	1.07
70	994	626	1.59	708	626	1.13	758	626	1.21	994	708	1.40	765	665	1.15
80	835	621	1.34	713	621	1.15	765	621	1.23	835	711	1.74	765	664	1.15
90	864	615	1.40	720	615	1.17	801	615	1.30	864	713	1.21	801	675	1.19
100	888	604	1.47	735	604	1.22	839	604	1.39	888	725	1.22	839	656	1.28

3.4. Electronic properties

As is well known, the band structure provides important information concerning the electronic and optical properties of materials. The obtained band structures with DFT and HSE06 and the total and partial density of states (PDOS) of *t*P40 carbon at zero pressure are illustrated in Fig. 6. The dashed line in Fig. 6 represents the Fermi level. The valence band maximum (VBM) is located at the Γ point, and the conduction band minimum (CBM) is located between the Γ point and Z point, which indicates that the *t*P40 carbon presents an indirect semiconducting character. The band gap calculated by DFT is 3.088 eV. As is well known, the band gap calculated by density functional theory is usually underestimated by 30%–50%. Therefore, the band gap of *t*P40 carbon with HSE06 hybrid functional is 4.130 eV. To obtain more information about the electronic band structure, the partial density of states of *t*P40 carbon is shown in Fig. 6(c). It can be noted that the distribution disciplines of these five atoms in different energy ranges are different. For C1, C2, and C3 atoms, the main contribution comes from the s orbital with energy ranging from −23 eV to −20 eV, the contribution of the s orbital is very small compared with the p orbital with energy in a range from −21 eV to Fermi energy, and the contribution from the p orbital is great compared with that from the s orbital in an energy range from 4 eV to 8 eV. For C4 atom, the density of states (DOS) can be divided into three parts: the lower energy part (−23 eV to −15 eV) where the peak mainly originates from the s orbital, the part where the states from −15 eV to Fermi energy are mainly due to the contribution of the p orbital, and the part where the peak appears on condition that the band DOS (4 eV to 8 eV) of the DOS is mainly due to the contribution of the p orbital. Regarding the DOS of C5 atom, the contribution from the p orbital is very small in the lowest band (−23 eV to −12.5 eV), the main contribution comes from the p orbital in the middle band (−12.5 eV to 0 eV), and the contribution from the p orbital is great compared with that from the s orbital in the upper band (4 eV to 8 eV). The DOS for *t*P40 carbon at zero pressure can be summarized as follows: (i) in the energy range below −12.5 eV, the contribution from the s orbital of the carbon atoms is larger than that from the p orbital; (ii) the peak present in the energy part (−12.5 eV to 8 eV) of the DOS mainly originates from the p orbital; (iii) the peak present in the energy part (4 eV to 8 eV) of the DOS mainly originates from the p orbital of C1, C3, C4, and C5, while the contribution of p orbital electron of C2 atom is smaller than that of carbon atom at other positions.

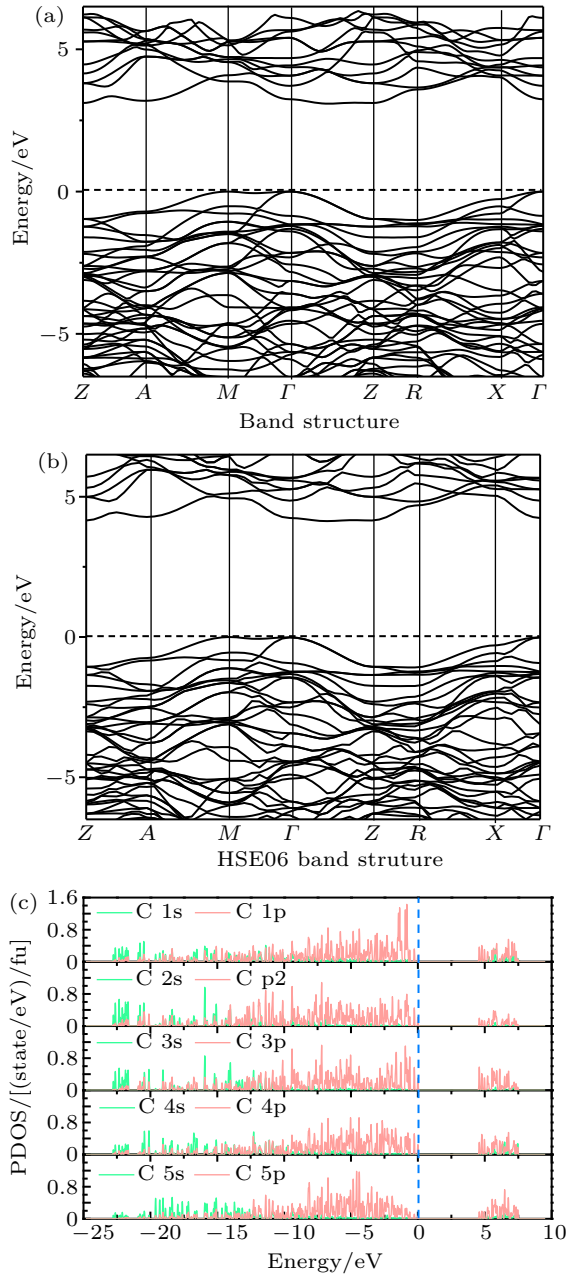


Fig. 6. Electronic band phases according to (a) DFT, (b) HSE06, and (c) DOS for *t*P40 carbon at zero pressure.

4. Conclusions

In this work, a new carbon allotrope *t*P40 carbon is theoretically predicted, and its structural properties, elastic properties, and anisotropy are investigated with first-principles calculations. By studying the elastic constants and phonon spectra, the *t*P40 carbon is found to be stable mechanically and dynamically. The *t*P40 carbon is brittle in a pressure range from 0 GPa to 60 GPa, but becomes ductile when the pressure exceeds 70 GPa. The obtained bulk modulus, shear modulus, and Young's modulus of *t*P40 carbon are 259 GPa, 234 GPa, and 540 GPa, respectively, which are larger than those of C72. The hardness of *t*P40 carbon is 44.0 GPa, indicating that the *t*P40 carbon can be considered to be a superhard material. The directional dependence of shear modulus, Young's modulus, Poisson's ratio, and the X_{max}/X_{min} indicate that the *t*P40 carbon shows elastic anisotropy. Comparing with diamond, the anisotropy in shear modulus and Young's modulus of *t*P40 carbon are larger, but in the Poisson's ratio, *t*P40 carbon exhibits smaller elastic anisotropy. The band structure of *t*P40 carbon indicates that it is an indirect band gap with a 4.130-eV band gap within HSE06, indicating that the *t*P40 carbon is a semiconductor material with an indirect and wider band gap.

References

[1] Xing M, Li B, Yu Z and Chen Q 2015 *J. Mater. Sci.* **50** 7104
[2] Zhang W, Chai C, Fan Q, Song Y and Yang Y 2020 *ChemNanoMat* **6** 139
[3] Wang J T, Chen C, Mizuseki H and Kawazoe Y 2018 *Phys. Chem. Chem. Phys.* **20** 7962
[4] Zhang W, Chai C, Song Y, Fan Q and Yang Y 2020 *J. Phys.: Condens. Matter* **32** 355701
[5] Fan Q Y, Wang H, Song Y X, Zhang W and Yun S N 2020 *Comput. Mater. Sci.* **178** 109634
[6] Cheng J, Zhang Q 2020 *Materials* **13** 2079
[7] Wei Q, Zhao C Y, Zhang M G, Yan H Y, Zhou Y J and Yao R H 2018 *Phys. Lett. A* **382** 1685
[8] Wang J T, Weng H, Nie S, Fang Z, Kawazoe Y and Chen C 2016 *Phys. Rev. Lett.* **116** 195501
[9] Li Z, Hu M, Ma M, Gao Y, Xu B, He J, Yu D, Tian Y and Zhao Z 2016 *Carbon* **105** 151
[10] Lv Y, Wang H, Guo Y, Jiang B and Cai Y 2018 *Comput. Mater. Sci.* **144** 170
[11] Yang X, Yao M, Wu X, Liu S, Chen S, Yang K, Liu R, Cui T, Sundqvist B and Liu B 2017 *Phys. Rev. Lett.* **118** 245701
[12] He C, Zhang C, Xiao H, Meng L and Zhong J 2017 *Carbon* **112** 91
[13] Xing M J, Li B H, Yu Z T and Chen Q 2015 *Commun. Theor. Phys.* **64** 237
[14] Zhao C X, Niu C Y, Qin Z J, Ren X Y, Wang J T, Cho J H and Jia Y 2016 *Sci. Rep.* **6** 21879
[15] Fan Q, Zhao Y, Yu X, Song Y, Zhang W and Yun S 2020 *Diamond Relat. Mater.* **106** 107831
[16] Li Z, Chen J, Nie S, Xu L, Mizuseki H, Weng H and Wang J T 2018 *Carbon* **133** 39
[17] Cui H J, Yan Q B, Sheng X L, Wang D L, Zheng Q R and Su G 2017 *Carbon* **120** 89
[18] Zhang W, Chai C, Fan Q, Song Y and Yang Y 2020 *Materials* **13** 1926
[19] Niu H, Chen X Q, Wang S, Li D, L. Mao W and Li Y 2012 *Phys. Rev. Lett.* **108** 135501
[20] Liu L, Hu M, Zhao Z, Pan Y and Dong H 2020 *Carbon* **158** 546
[21] Amsler M, Flores-Livas J A, Lehtovaara L, Balima F, Ghasemi S A, Machon D, Pailhès S, Willand A, Caliste D, Botti S, Miguel A S, Goedecker S and Marques M A L 2012 *Phys. Rev. Lett.* **108** 065501
[22] Xu Y, Lu Y, Zhu X and Wang M 2018 *RSC Adv.* **8** 1846
[23] Niu C Y, Wang X Q and Wang J T 2014 *J. Chem. Phys.* **140** 054514
[24] Zhang W, Chai C, Fan Q, Song Y and Yang Y 2019 *J. Appl. Phys.* **126** 145704
[25] Zhang Z G, Liu H Y and Zhang M 2014 *Europhys. Lett.* **108** 46006
[26] Zhao C X, Niu C Y, Qin Z J, Ren X Y, Wang J T, Cho J H and Jia Y 2016 *Sci. Rep.* **6** 21879
[27] Wei Q, Zhang Q, Zhang M G, Yan H Y, Guo L X and Wei B 2018 *Front. Phys.* **13** 136105
[28] Umemoto K, Wentzcovitch R M, Saito S and Miyake T 2010 *Phys. Rev. Lett.* **104** 125504
[29] Wang J T, Chen C F and Kawazoe Y 2012 *Phys. Rev. B* **85** 033410
[30] Yang X, Lv C, Liu S, Zang J, Qin J, Du M, Yang D, Li X, Liu B and Shan C X 2020 *Carbon* **156** 309
[31] Zhang X X, Wang Y C, Lv J, Zhu C Y, Li Q, Zhang M, Li Q and Ma Y 2013 *J. Chem. Phys.* **138** 114101
[32] Xing M J, Li X Z, Yu S J and Wang F Y 2017 *Commun. Theor. Phys.* **68** 395
[33] Li D, Tian F B, Chu B H, Duan D F, Wei S L, Lv Y Z, Zhang H D, Wang L, Lu N, Liu B B and Cui T 2015 *J. Mater. Chem. A* **3** 10448
[34] Sheng X L, Yan Q B, Ye F, Zheng Q R and Su G 2011 *Phys. Rev. Lett.* **106** 155703

[35] Wang J Q, Zhao C X, Niu C Y, Sun Q and Jia Y 2016 *J. Phys.: Condens. Matter* **28** 475402
[36] Li X and Xing M 2020 *Mater. Chem. Phys.* **242** 122480
[37] Zhang J, Wang R, Zhu X, Pan A, Han C, Li X, Dan Z, Ma C, Wang W, Su H and Niu C 2017 *Nat. Commun.* **8** 683
[38] Chen X Q, Niu H Y, Li D Z and Li Y Y 2011 *Intermetallics* **19** 1275
[39] Lyakhov A O and Oganov A R 2011 *Phys. Rev. B* **84** 92103
[40] Shi X, He C, Pickard C J, Tang C and Zhong J 2018 *Phys. Rev. B* **97** 014104
[41] He C, Shi X, Clark S J, Li J, Pickard C J, Ouyang T, Zhang C, Tang C and Zhong J 2018 *Phys. Rev. Lett.* **121** 175701
[42] Hoffmann R, Kabanov A A, Golov A A and Proserpio D M 2016 *Angew. Chem. Int. Ed.* **55** 10962
[43] O'Keeffe M, Yaghi O M and Ramsden S, Reticular Chemistry Structure Resource, Australian National University Supercomputer Facility, http://rcsr.anu.edu.au/, accessed 5th March 2013
[44] O'Keeffe M, Peskov M A, Ramsden S and Yaghi O M 2008 *Chem. Res.* **41** 1782
[45] Pan Y, Xie C, Xiong M, Ma M, Liu L, Li Z, Zhang S, Gao G, Zhao Z, Tian Y, Xu B and He J 2017 *Chem. Phys. Lett.* **689** 68
[46] Hohenberg P and Kohn W 1964 *Phys. Rev.* **136** B864
[47] Kohn W and Sham L J 1956 *Phys. Rev.* **140** A1133
[48] Clark S J, Segall M D, Pickard C J, Hasnip P J, Probert M I J, Refson K and Payne M C 2005 *Z. Kristallogr* **220** 567
[49] Perdew J P, Burke K and Ernzerhof M 1996 *Phys. Rev. Lett.* **77** 3865
[50] Ceperley D M and Alder B J 1980 *Phys. Rev. Lett.* **45** 566
[51] Krukau A V, Vydrov O A, Izmaylov A F and Scuseria G E 2006 *J. Chem. Phys.* **125** 224106
[52] Vanderbilt D 1990 *Phys. Rev. B* **41** 7892
[53] Pfrommer B G, Côté M, Louie S G and Cohen M L 1997 *J. Comput. Phys.* **131** 233
[54] Baroni S, de Gironcoli S, dal Corso A and Giannozzi P 2001 *Rev. Mod. Phys.* **73** 515
[55] Ma Z, Han Z, Liu X, Yu X, Wang D and Tian Y 2017 *Nanomaterials* **7** 3
[56] Wei Q, Zhang Q, Yan H Y and Zhang M G 2017 *J. Mater. Sci.* **52** 2385
[57] Ma J L, Song D L, Wu Y L, Fu Z F, Zhou J P, Liu P, Zhu X and Wei Q 2020 *Phys. Lett. A* **384** 126325
[58] Xing M, Li B, Yu Z and Chen Q 2016 *Eur. Phys. J. B* **89** 9
[59] Fan Q, Wei Q, Chai C, Yan H, Zhang M, Lin Z, Zhang Z, Zhang J and Zhang D 2015 *J. Phys. Chem. Solids* **79** 89
[60] Petrescu M L 2004 *Diamond Relat. Mater.* **13** 1848
[61] Mouhat F and Coudert F X 2014 *Phys. Rev. B* **90** 224104
[62] Grimsditch M, Zouboulis E S and Polian A 1994 *J. Appl. Phys.* **76** 832
[63] Hill R 1952 *Proc. Phys. Soc. London* **65** 349
[64] Fan Q, Zhang W, Song Y, Zhang W and Yun S 2020 *Semicond. Sci. Technol.* **35** 055012
[65] Fan Q, Niu R, Zhang W, Zhang W, Ding Y and Yun S 2019 *ChemPhysChem* **20** 128
[66] Pugh S F 1954 *Philos. Mag.* **45** 823
[67] Anderson O L 1963 *J. Phys. Chem. Solids* **24** 909
[68] Panda K B and Ravi K S 2006 *Comput. Mater. Sci.* **35** 134
[69] Fan Q, Wei Q, Yan H, Zhang M, Zhang Z, Zhang J and Zhang D 2014 *Comput. Mater. Sci.* **85** 80
[70] Fan Q, Chai C, Wei Q, Wong K, Liu Y and Yang Y 2018 *J. Mater. Sci.* **53** 2785
[71] Fan Q, Duan Z, Song Y, Zhang W, Zhang Q and Yun S 2019 *Materials* **12** 3589
[72] Connétable D and Thomas O 2009 *Phys. Rev. B* **79** 094101
[73] Ravindran P, Fast L, Korzhavyi P A, Johansson B, Wills J and Eriksson O 1998 *J. Appl. Phys.* **84** 4891
[74] Marmier A, Lethbridge Z A D, Walton R I, Smith C W, Parker S C and Evans K E 2010 *Comput. Phys. Commun.* **181** 2102
[75] Ma Z Y, Wang P, Yan F, Shi C L and Tian Y 2019 *Chin. Phys. B* **28** 036101
[76] Zhang Q, Zou Y, Fan Q and Yang Y 2020 *Materials* **13** 1280
[77] Hu W C, Liu Y, Li D J, Zeng X Q and Xu C S 2014 *Comput. Mater. Sci.* **83** 27